c-Myc-regulated RPLP0 via the ROS-mediated JAK2/STAT3 positive feedback loop facilitates hepatocellular carcinoma malignancy progression

YANQIU MENG[1*], LEBIN YUAN[2*], GANGRUI MENG[3*], HONGXIANG HUANG[4], XIANBIN HUANG[1], XINPING XU[5] and XIAODONG PENG[1]

[1]Department of Oncology, The First Affiliated Hospital, Jiangxi Medical College, Nanchang University, Nanchang, Jiangxi 330006, P.R. China; [2]Department of Thyroid and Breast Surgery, Affiliated Hospital of Hubei University of Arts and Science, Xiangyang Central Hospital, Xiangyang, Hubei 441000, P.R. China; [3]Department of General Surgery, First Clinical College, Hubei University of Medicine, Shiyan, Hubei 442000, P.R. China; [4]Department of Oncology, Ganzhou Hospital-Nanfang Hospital, Southern Medical University, Ganzhou, Jiangxi 341000, P.R. China; [5]Jiangxi Provincial Key Laboratory of Respiratory Diseases, Jiangxi Institute of Respiratory Diseases, The Department of Respiratory and Critical Care Medicine, Jiangxi Clinical Research Center for Respiratory Diseases, The First Affiliated Hospital, Jiangxi Medical College, Nanchang University, Nanchang, Jiangxi 330006, P.R. China

Received June 26, 2025; Accepted October 3, 2025

DOI: 10.3892/ijo.2025.5826

Abstract. Hepatocellular carcinoma (HCC) continues to rank as a predominant contributor to cancer-related mortality on a global scale, attributed to its insidious onset and unfavorable prognosis. The ribosomal protein lateral stalk subunit P0 (RPLP0) has recently gathered widespread attention as a crucial factor in the pathological progression of various neoplasms; however, its exact role in HCC remains inadequately defined. Consequently, the present study endeavored to shed light on the function and mechanistic underpinnings of RPLP0 in HCC and assess its clinical significance and potential as a therapeutic target. qPCR and western blot analyses indicated that RPLP0 was markedly upregulated in HCC, with its elevated levels correlating with poorer survival outcomes. Silencing RPLP0 expression suppressed the proliferative, invasive, migratory, and epithelial-mesenchymal transition (EMT) abilities of HCC cells, while concurrently promoting apoptosis, autophagy, and G_2/M cell cycle arrest, as evidenced by CCK-8, colony formation, Transwell assays and flow cytometry analysis, respectively. Moreover, the findings revealed that RPLP0 downregulation mediated the suppression of the JAK2/STAT3 pathway through reactive oxygen species (ROS) accumulation, which in turn downregulated c-Myc expression. Furthermore, chromatin immunoprecipitation and dual luciferase assays demonstrated that c-Myc directly bound to the promoter sequence of RPLP0, thereby augmenting its transcriptional activity. In summary, the current study highlighted that RPLP0 establishes a feedback circuit with c-Myc by facilitating JAK2/STAT3 pathway activation through suppressing ROS levels, while c-Myc reciprocally activates RPLP0, forming a regulatory circuit loop that drives HCC progression. Thus, targeting the c-Myc/RPLP0/ROS/JAK2/STAT3 axis emerges as a promising therapeutic strategy for the management of HCC.

Correspondence to: Professor Xinping Xu, Jiangxi Provincial Key Laboratory of Respiratory Diseases, Jiangxi Institute of Respiratory Diseases, The Department of Respiratory and Critical Care Medicine, Jiangxi Clinical Research Center for Respiratory Diseases, The First Affiliated Hospital, Jiangxi Medical College, Nanchang University, 1519 Dongyue Avenue, Nanchang, Jiangxi 330006, P.R. China
E-mail: xinpingxu@ncu.edu.cn

Professor Xiaodong Peng, Department of Oncology, The First Affiliated Hospital, Jiangxi Medical College, Nanchang University, 1519 Dongyue Avenue, Nanchang, Jiangxi 330006, P.R. China
E-mail: pxddhbb@163.com

*Contributed equally

Key words: hepatocellular carcinoma, c-Myc, ribosomal protein lateral stalk subunit P0, reactive oxygen species, JAK2/STAT3

Introduction

Hepatocellular carcinoma (HCC) constitutes ~80% of liver malignancies, making it the third most lethal cancer and the sixth most prevalent malignancy worldwide (1,2). HCC pathogenesis and progression are influenced by numerous factors (3,4). Despite recent advances in surgical resection, targeted pharmacotherapy, precision radiotherapy and immunotherapy, a significant proportion of HCC patients face unsatisfactory survival outcomes, attributable to the inherently aggressive nature of HCC (5-7). Hence, there is a pressing need to investigate key molecules involved in HCC development and

identify associated diagnostic markers and treatment targets for enhancing patient prognosis.

The ribosomal protein lateral stalk subunit P0 (RPLP0), an integral component of the RPLP family and a key ribosomal protein in the 60S subunit, markedly influences cell fate determination and is intricately involved in tumorigenesis. RPLP0 expression is markedly upregulated in gastric, breast, ovarian, endometrial and cervical carcinomas and its overexpression is associated with suboptimal survival outcomes in patients (8-11). Wang *et al* (12) discovered that RPLP0 interacts with NONO independently of the ribosome and can anchor to damaged DNA, thereby promoting the autophosphorylation of DNA-dependent protein kinase at the Thr2609 site, enhancing the repair of double-strand breaks and conferring resistance to radiotherapy. The knockdown of RPLP0 has been observed to enhance autophagy, a cellular degradation mechanism targeting cytoplasmic components (13,14) and to trigger G_2/M cell cycle arrest in breast cancer (9). Although RPLP0 abnormal expression markedly affects tumor progression, its pathophysiological role in HCC remains to be elucidated.

While prior research has established the involvement of RPLP0 in HCC development (15), the specific regulatory pathways and mechanisms governing its regulation remain underexplored. Therefore, the present study performed an in-depth analysis to unravel the intricate mechanisms underlying the formation of regulatory loops through which RPLP0 contributes to HCC progression. By integrating multiple transcriptomic datasets and clinical data, coupled with rigorous *in vitro* and *in vivo* experimental procedures, a clinically relevant RPLP0 profile was established in HCC. These results collectively position RPLP0 as a prognostic marker and therapeutic target, representing a significant advancement in our understanding of HCC biology and offering a promising strategy for improving clinical outcomes.

Materials and methods

Cell culture. The cell lines THLE-2, SNU-182, Li-7, Huh-7, PLC/PRF/5, MHCC97-H and HCCLM3 were sourced from the Chinese Academy of Sciences and maintained at 37˚C with 5% CO_2 in a humidified incubator. THLE-2 cells were cultured in BEGM (Gibco; Thermo Fisher Scientific, Inc.), SNU-182 cells were propagated in RPMI 1640 (Gibco; Thermo Fisher Scientific, Inc.), Li-7 cells were maintained in MEM (Gibco; Thermo Fisher Scientific, Inc.), and Huh-7, PLC/PRF/5, MHCC97-H, and HCCLM3 cells were grown in DMEM (Gibco; Thermo Fisher Scientific, Inc.). Each of these media was supplemented with 10% FBS (Gibco; Thermo Fisher Scientific, Inc.), and the incubator was supplied by Gibco (Thermo Fisher Scientific, Inc.). For subsequent experiments, Huh-7 and MHCC97-H cell lines were selected based on their demonstrated phenotypic stability and experimental reproducibility, making them suitable for detailed investigation, as well as their well-characterized properties in HCC research (16). The properties of the cell lines are given in Table SI.

Tissue samples. Between October 2024 and February 2025, a cohort of 44 paired specimens, comprising tumor and adjacent non-tumor tissues (designated at sites >5 cm from the tumor margin), was procured from patients diagnosed with HCC (clinicopathological features are provided in Table SII). The median age was 62 years (range, 36-78). These tissue specimens were exclusively sourced from individuals with untreated primary HCC who had provided their written informed consent. The study was performed in strict compliance with the Declaration of Helsinki and received approval from the Institutional Review Board under protocol number (2024) CDYFYYLK (07-004).

Bioinformatics analysis. The expression profile and clinical significance of RPLP0 were systematically evaluated using an integrative bioinformatics approach that used data from multiple high-throughput repositories. Specifically, this analysis incorporated comprehensive datasets from The Cancer Genome Atlas (TCGA; https://portal.gdc.cancer.gov/), which includes 371 HCC samples and 50 non-tumor controls; the Genotype-Tissue Expression (GTEx) project (https://gtexportal.org/home/index.html), encompassing 110 healthy liver tissues; the Gene Expression Profiling Interactive Analysis (GEPIA)2 repository (http://gepia2.cancer-pku.cn/#index); and the Gene Expression Omnibus (GEO) platform (https://www.ncbi.nlm.nih.gov/), using datasets GSE57957, GSE36411, GSE39791 and GSE76427. R software (version 4.3.2 https://cran.r-project.org/) was used to assess correlations between RPLP0 expression, histological grading and tumor staging based on TCGA data. Additionally, pathway enrichment analysis was performed by stratifying samples into high and low RPLP0 expression groups. Transcription factors and specific promoter sequences for RPLP0 were identified using predictive tools such as the Cistrome Data Browser (http://cistrome.org/db/#/) and JASPAR databases (https://jaspar.elixir.no/).

Reverse transcription-quantitative (RT-q) PCR. Following the respective manufacturers' instructions, RNA was extracted with TRIzol® reagent (Invitrogen; Thermo Fisher Scientific, Inc.), then reverse transcription and qPCR were performed using the cDNA Synthesis SuperMix and qPCR SYBR Green Master Mix, respectively (both from Shanghai Yeasen Biotechnology Co., Ltd.). The thermocycling protocol consisted of an initial denaturation at 95˚C for 2 min, followed by 40 cycles of 95˚C for 10 sec and 60˚C for 30 sec. Melting curve analysis was carried out as follows: 95˚C for 15 sec, 60˚C for 1 min, and 95˚C for 15 sec. Relative mRNA expression levels were quantified using the comparative $2^{-\Delta\Delta Cq}$ method (17), with GAPDH serving as the endogenous control. All experiments were independently repeated three times. Primer sequences are listed in Table SIII.

Western blotting. To ensure high-fidelity protein extraction, samples were lysed using RIPA buffer (Invitrogen; Thermo Fisher Scientific, Inc.) supplemented with protease and phosphatase inhibitors to preserve post-translational modifications and prevent protein degradation. The extracted proteins were quantified using a BCA kit (Thermo Fisher, Inc.). Subsequently, depending on the molecular weight of the proteins of interest, SDS-PAGE electrophoresis was executed on gels with either 10 or 12.5% polyacrylamide concentration. Each lane was loaded with a standardized amount of total protein (20 μg). Following electrophoresis, proteins were transferred to 0.45 μm PVDF membranes (MilliporeSigma) using a wet

transfer system. The membrane was then blocked with 5% non-fat milk in TBST (0.1% Tween-20) for 1 h at room temperature to prevent non-specific binding. The membrane was incubated overnight at 4˚C with primary antibodies specific to the proteins of interest, diluted according to the manufacturer's recommendations. After washing with TBST (0.1% Tween-20), the membrane was incubated with an HRP-conjugated secondary antibody for 1 h at room temperature. The target proteins were ultimately clearly and precisely detected using an ECL detection system (Bio-Rad Laboratories, Inc.). The resulting band intensities were quantified by densitometry using ImageJ software (version 1.53m; National Institutes of Health). Antibodies details are in Table SIV.

Immunohistochemistry. Tumor specimens were fixed in 10% neutral buffered formalin for 48 h at room temperature, followed by routine dehydration through a graded ethanol series and embedding in paraffin. Consecutive sections were cut at a thickness of 4 μm. Following deparaffinization and rehydration, antigen retrieval was performed using citrate buffer (pH 6.0). Endogenous peroxidase activity was quenched by incubation with 3% hydrogen peroxide for 10 min. Sections were then permeabilized with 0.2% Triton X-100 and blocked with 5% bovine serum albumin (BSA; both from Beyotime Institute of Biotechnology) for 1 h at room temperature. After being placed in contact with the primary antibody at room temperature for 2 h to promote optimal antigen-antibody binding, the sections underwent a 30-min incubation at 37˚C with the secondary antibody. Antibodies details are in Table SIV. Chromogenic visualization was achieved using a 0.02% diaminobenzidine (DAB) solution for 5 min, providing clear staining of target proteins. Subsequently, the sections were counterstained with hematoxylin for 30 sec to provide nuclear contrast at room temperature, dehydrated through graded alcohols, cleared in xylene, and air-dried. The slides were then mounted and examined under light microscopy for detailed immunohistochemical analysis.

Small interfering (si)RNA, plasmid transfection and short hairpin (sh)RNA. In the present study, the target cell lines, Huh7 and MHCC97-H cells, were seeded in 6-well plates. Cells were subjected to transfection using siRPLP0 (150 nM; Shanghai GenePharma Co., Ltd.) and pECMV-RPLP0 (2.5 μg; MiaoLing Biology) to knock down and overexpress RPLP0, respectively, using Lipofectamine® 3000 transfection reagent (Thermo Fisher Scientific, Inc.) according to the manufacturer's instructions. Parallel transfections with si-NC (150 nM) or oe-NC (2.5 μg) served as negative controls. A c-Myc-specific siRNA (150 nM; Shanghai GenePharma Co., Ltd.) and the plasmid pCMV-c-Myc (2.5 μg; MiaoLing Biology) were employed to knock down and overexpress c-Myc, respectively. The transfection mixture was incubated with the cells for 6 h at 37˚C, after which it was replaced with fresh complete medium. Subsequent functional experiments were typically performed 48 h post-transfection. To achieve stable RPLP0 knockdown, MHCC97-H cells were transduced with shRNA specifically targeting RPLP0 (shRPLP0; Hanbio Biotechnology Co., Ltd.) at a multiplicity of infection (MOI) of 50. Following a 48-h incubation at 37˚C, stable transductants were selected and maintained in complete medium supplemented with 2.0 μg/ml puromycin (Biosharp Life Sciences) for two weeks. Detailed sequences are listed in Table SV.

Cell proliferation assay. After successful transfection, the cells were trypsinized and subsequently resuspended in single-cell suspensions. For CCK-8 assays, 1,500 cells was dispensed into each well of a 96-well plate and absorbance was measured at specific intervals. In the colony-forming efficiency test, 1,000 isolated cells were uniformly distributed in each well of 6-well plates. After 12 days, colonies became macroscopically visible and they were sequentially fixed, stained, air-dried, and photographed.

Transwell assay. Cells were transfected for 48 h, after which 200 μl of a suspension containing $4x10^4$ cells was introduced into the upper chamber of a Matrigel-coated (incubated at 37˚C for 2 h for gel formation) Transwell system featuring 8 μm pores. Meanwhile, the lower chamber was replenished with 600 μl of DMEM supplemented with 20% FBS. At 48 h, samples were fixed with 4% paraformaldehyde for 30 min at room temperature, stained with 0.1% crystal violet for 20 min at room temperature and imaged under a light microscope. For migration assays, Transwell chambers that had not been pretreated with Matrigel were used.

Apoptosis and cell cycle assay. Apoptosis and cell cycle distribution were analyzed using the Annexin V-PE/7-AAD apoptosis kit and the Cell Cycle Staining Kit (MultiSciences Biotech Co., Ltd.), respectively, according to the manufacturer's guidelines. After staining at room temperature for 30 min in the dark, the samples were analyzed using a flow cytometer (Beckman Coulter, Inc.). Data were processed with FlowJo software (version 10.1; BD FlowJo) (18). The apoptotic rate was defined as the combined percentage of early and late apoptotic cells in the total population.

Reactive oxygen species (ROS) assay. Intracellular ROS levels were determined employing the Reactive Oxygen Species Assay Kit (Beyotime Institute of Biotechnology) according to the manufacturer's instructions. Cells underwent staining with 1X Hoechst for 20 min at ambient temperature and subsequently were incubated in the dark at 37˚C with 10 μM DCFH-DA for 30 min. After incubation, the excess DCFH-DA was removed by washing the cells three times with serum-free culture medium to minimize non-specific extracellular fluorescence. The assessment of ROS levels was performed using either fluorescence microscopy (Leica Microsystems GmbH) or a flow cytometer (CytoFLEX; Beckman Coulter, Inc.). During flow cytometry, the excitation and emission wavelengths were set at 488 nm and 525 nm, respectively, and a total of 10,000 events were acquired per sample. Data were analyzed using FlowJo software (version 10.1; BD FlowJo) (18).

Monodansylcadaverine (MDC) staining. To assess the levels of intracellular autophagosomes, the present study used an MDC staining kit (Beyotime Institute of Biotechnology). Cells underwent a 20-min incubation period in dim conditions at ambient temperature with 1X Hoechst solution. This was followed by another 30 min of incubation at 37˚C in 500 μl of 1X MDC solution, with darkness maintained throughout. After washing

three times with assay buffer, the cells were examined under a fluorescence microscope (Leica Microsystems GmbH).

Transmission electron microscopy (TEM). The collected cells were fixed with a specialized electron microscopy fixative (Wuhan Servicebio Technology Co., Ltd.) at 4˚C overnight, followed by dehydration through an ethanol gradient. Subsequently, the samples underwent infiltration with propylene oxide and were embedded in resin using a progressive temperature protocol (37˚C for 12 h, 45˚C for 12 h, and 60˚C for 24 h). Ultrathin sections (70 nm) were prepared using an ultramicrotome, then double-stained with uranyl acetate for 15 min and lead citrate for 5 min at room temperature. After overnight drying, the sections were examined utilizing a transmission electron microscope (Hitachi High-Technologies Corporation).

Chromatin immunoprecipitation (ChIP) assay. The ChIP procedure was performed in strict accordance with the guidelines furnished by the ChIP assay kit procured from Cell Signaling Technology, Inc. Cells grown in 10 cm dishes at 80-90% confluence were initially fixed with 1% formaldehyde for 10 min at room temperature. After quenching with 125 mM glycine, cells were lysed and the chromatin was fragmented using a non-contact ultrasonicator (Little Scientific Instruments Co., Ltd.) set at 100% power for 25 min with cycles of 10 sec ON and 5 sec OFF at 4˚C, yielding DNA fragments of 200-600 bp. A 10 μl aliquot of the lysate was reserved and stored at -80˚C for subsequent use as an input. Next, 500 μl of lysate underwent immunoprecipitation through overnight incubation at 4˚C using protein A/G beads with 5 μl of either anti-c-Myc (4 μg) or anti-IgG antibodies (4 μg). The beads were washed sequentially with low salt, high salt and LiCl wash buffers provided in the ChIP assay kit. The purified DNA fragments subsequently underwent qPCR. Purified DNA fragments were amplified via PCR using reagents acquired from Vazyme Biotech Co., Ltd. and the following cycling conditions: initial denaturation at 95˚C for 3 min; 35 cycles of denaturation at 95˚C for 15 sec, annealing at 60˚C for 15 sec, and extension at 72˚C for 30 sec; and final extension at 72˚C for 5 min. PCR products were separated on 2% agarose gels and visualized with GelStain (Bio-Rad Laboratories, Inc.) under UV illumination. The specific primer sequences used for qPCR in the ChIP assay are presented in Table SVI.

Dual luciferase assay. The promoter sequences of both the native (wild-type; WT) and altered (mutant; MUT) RPLP0 were cloned into pGL4 plasmids (Promega Corporation). Afterward, cells seeded in 24-well plates at 70-80% confluence were co-transfected using Lipofectamine® 3000 reagent (Thermo Fisher Scientific, Inc.) with either pGL4-RPLP0-WT or pGL4-RPLP0-MUT, together with the pGL4.74 internal control plasmid and either pCMV-c-Myc or the corresponding empty vector. After a 48-h incubation period, luciferase activity was quantified employing the Dual Luciferase Assay Kit (Promega Corporation).

Xenograft tumor model. A subcutaneous xenograft model was generated using 16 BALB/c nude female mice (4-5 weeks old, 15-16 g; Sibeifu Laboratory Animal Co. Ltd.) and maintained under strict SPF conditions (22±1˚C; relative humidity 50±10%; a 12/12-h light/dark cycle, and *ad libitum* access to sterilized food and water). Lentivirus-infected MHCC97-H cells, targeting shNC and shRPLP0, were successfully screened to establish stable cell lines. Subsequently, an inoculation of $6x10^6$ cells, comprising either shNC or shRPLP0, was administered at the specified subcutaneous site in each mouse. The dimensions of the subcutaneous tumors were precisely assessed and recorded every four days. Tumor volume was calculated using the formula: length x $width^2$ x0.5. The largest tumor observed in the present study measured 10.82 mm in length and 7.28 mm in width, with a maximum volume of 286.72 mm^3. In compliance with animal ethics guidelines, tumor size was limited to a mean diameter of 20 mm and a volume of 2,000 mm^3. Sacrifice was via carbon dioxide (CO_2) inhalation at a chamber displacement rate of 30-50% per min prior to tumor excision, with mortality confirmed by absent heartbeat and respiration. Animal studies were performed following ethical guidelines and were approved by the Animal Ethics Committee (approval no. CDYFY-IACUC-202407QR259).

Statistical analysis. Data analysis was conducted using GraphPad Prism 9 (Dotmatics). For comparisons of RPLP0 mRNA expression between tumor and adjacent non-tumor tissues from HCC patients, a paired Student's t-test was applied. Other comparisons between two groups were conducted using an unpaired Student's t-test. For multiple group comparisons, one-way ANOVA followed by Bonferroni's post hoc test was applied. The Spearman correlation coefficient was determined to assess relationships between variables. Kaplan-Meier curves and log-rank tests were used to analyze survival prognosis. Data were presented as mean ± SEM. $P<0.05$ was considered to indicate a statistically significant difference.

Results

RPLP0 is markedly upregulated in HCC and its high expression is associated with poorer prognosis. Analyses based on the TCGA and GTEx databases demonstrated that RPLP0 transcriptome levels were markedly elevated in HCC samples (Fig. 1A). Consistent findings were observed in the GSE57957, GSE36411, GSE39791 and GSE76427 datasets, providing further validation of the heightened expression of RPLP0 in HCC (Fig. 1B). The GEPIA 2 database revealed that individuals with elevated RPLP0 levels experienced decreased overall survival (OS) and disease-free survival (DFS) rates (Fig. 1C and D). TCGA database analysis showed that high RPLP0 expression levels were associated with unfavorable histological grades and tumor stages (Fig. 1E and F). Furthermore, comparative studies of mRNA and protein levels in 44 matched tissues clearly indicated a marked elevation in RPLP0 in HCC (Fig. 1G and H). After stratifying samples by median RPLP0 expression, a Kaplan-Meier analysis demonstrated that higher RPLP0 expression was markedly associated with inferior outcomes in HCC patients (Fig. 1I). Immunohistochemical analysis of the collected samples further validated the upregulation of RPLP0 expression in HCC tissues (Fig. 1J). Compared with immortalized hepatocytes, RPLP0 expression was notably higher in HCC cell lines at both mRNA and protein levels

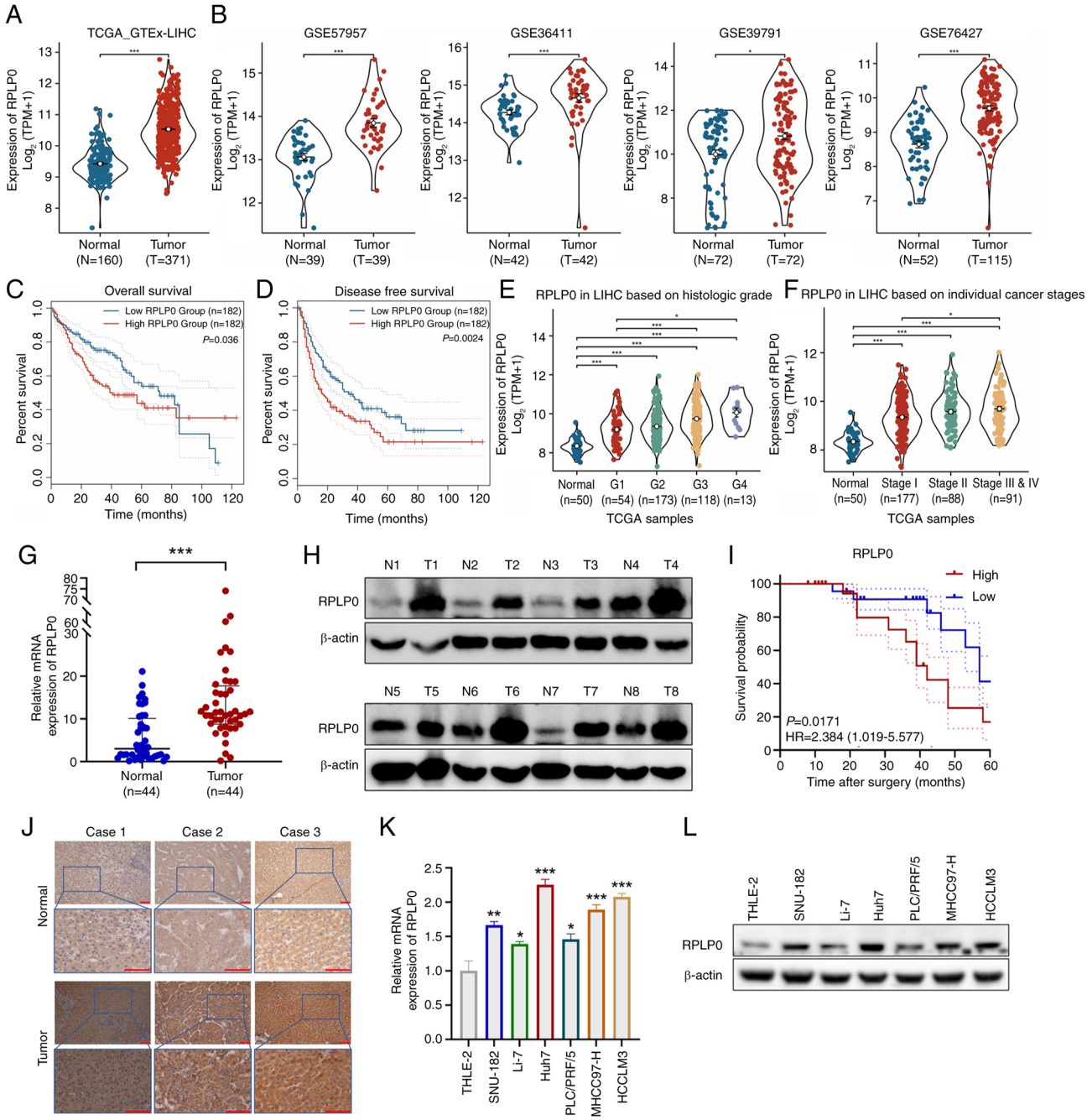

Figure 1. Elevated RPLP0 expression is associated with unfavorable survival outcomes in HCC. (A) RPLP0 expression levels derived from the TCGA_GTEx database. (B) Confirmation of RPLP0 expression in the GSE57957, GSE36411, GSE39791 and GSE76427 datasets. Association between RPLP0 expression status and (C) OS and (D) DFS among HCC patients in the GEPIA2 database. The relationship between RPLP0 expression and (E) histological grade and (F) cancer stage in the TCGA database. The expression levels of (G) mRNA and (H) protein for RPLP0 were analyzed in 44 paired HCC samples. (I) The influence of RPLP0 expression on the survival outcomes of HCC patients. (J) Immunohistochemical analysis of RPLP0 in HCC and adjacent non-cancerous tissues (scale bar, 100 μm). RPLP0 (K) mRNA and (L) protein levels were examined in immortalized hepatocytes and HCC cell lines. *P<0.05, **P<0.01, ***P<0.001. RPLP0, ribosomal protein lateral stalk subunit P0; HCC, hepatocellular carcinoma; TCGA, the cancer genome atlas; GTEx, the genotype-tissue expression; N, normal; T, tumor; GEO, gene expression omnibus; GEPIA2, gene expression profiling interactive analysis; OS, overall survival; DFS, disease-free survival.

(Fig. 1K and L). Overall, these results suggest that RPLP0 may be utilized as a diagnostic and prognostic biomarker in HCC.

RPLP0 downregulation suppresses the malignant phenotype of HCC cells, inducing apoptosis and G_2/M cell cycle arrest. To further explore the biological function of RPLP0 in HCC, its expression was modulated in Huh7 and MHCC97-H cell lines using siRPLP0 and oeRPLP0, respectively and their controls. This caused changes in RPLP0 levels at both the mRNA and protein (Fig. 2A-D) levels. The findings obtained through the CCK-8, colony formation efficiency test and Transwell assay showed that RPLP0 downregulation suppressed the proliferative, invasive and migratory potentials of HCC cells. By contrast, the upregulation of RPLP0 enhanced these cellular properties in HCC cells (Fig. 2E-G). Western blot analysis indicated that the siRPLP0 group exhibited markedly increased levels of E-cadherin in comparison to the si-NC

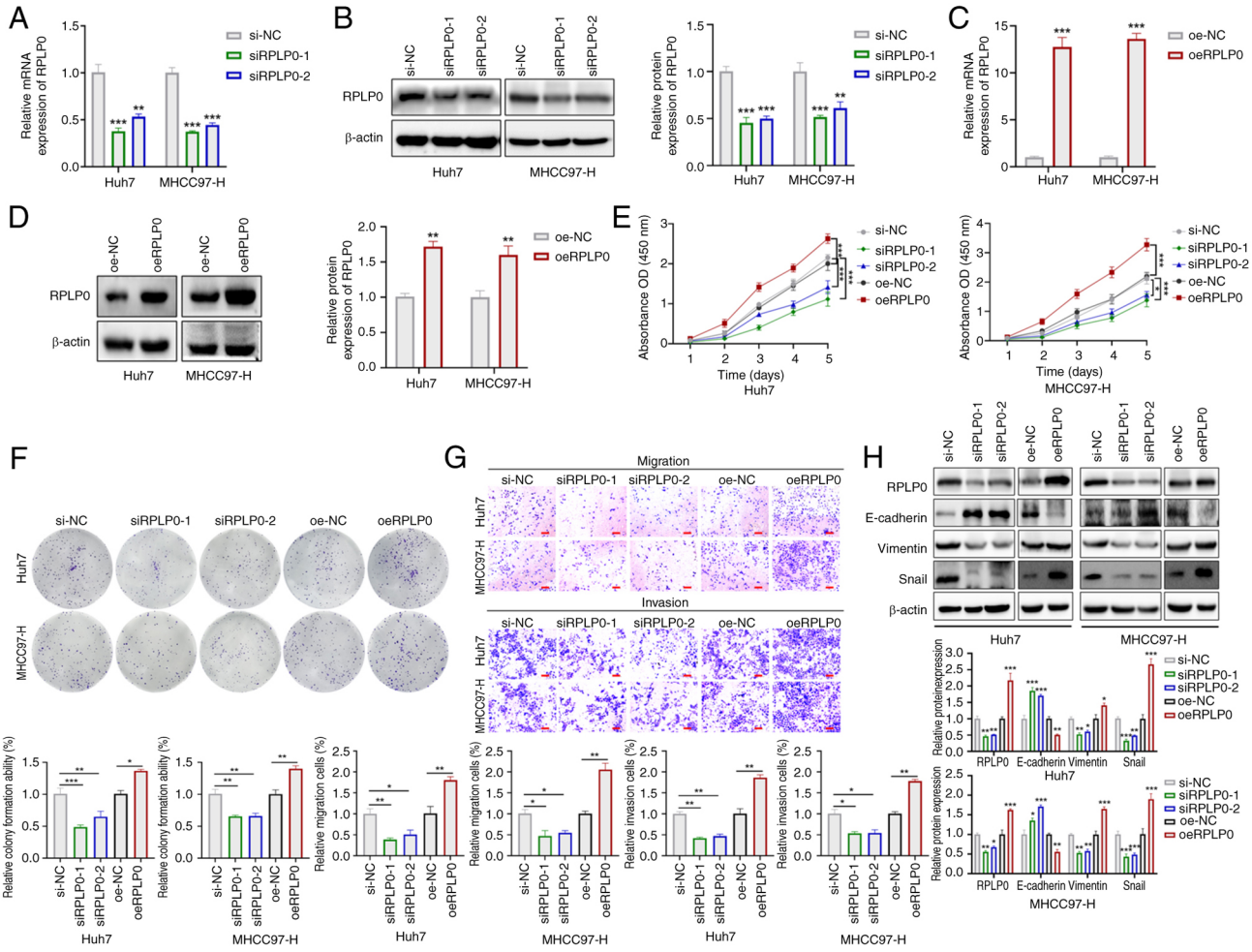

Figure 2. RPLP0 overexpression promotes malignant phenotypes in HCC cells. Alterations in mRNA and protein levels following (A and B) RPLP0 knockdown and (C and D) overexpression in HCC cells. (E) CCK-8, (F) colony formation and (G) Transwell assays were conducted to assess HCC cell proliferation, invasion and migration (scale bar, 150 μm). (H) EMT-related protein expression changes (E-cadherin, Vimentin and Snail) were observed in treated HCC cells. *P<0.05, **P<0.01, ***P<0.001. RPLP0, ribosomal protein lateral stalk subunit P0; HCC, hepatocellular carcinoma; CCK-8, cell counting kit-8; EMT, epithelial-mesenchymal transition.

group, accompanied by notably decreased levels of Vimentin and Snail. Conversely, the oeRPLP0 group demonstrated markedly reduced levels of E-cadherin in comparison to the oe-NC group, with concurrently elevated levels of Vimentin and Snail (Fig. 2H). Flow cytometry analysis indicated that downregulation of RPLP0 promoted apoptosis and mediated G_2/M cell cycle arrest, whereas upregulation of RPLP0 inhibited apoptosis and promoted G_2/M cell cycle transition (Fig. 3A-B). Subsequently, the influence of RPLP0 modulation on the expression patterns of proteins implicated in apoptosis and cell cycle regulation was examined. Western blot analysis showed that Poly (ADP-ribose) polymerase (PARP), Bcl-2 and Cyclin D1 levels were markedly decreased in the siRPLP0 group whereas cleaved (C-)PARP expression levels were elevated. Conversely, the oeRPLP0 group displayed a marked up-regulation in PARP, Bcl-2 and Cyclin D1 levels, accompanied by the downregulation of C-PARP expression (Fig. 3C). These findings conjointly indicate that the knockdown of RPLP0 delays malignant progression in HCC cells.

RPLP0 knockdown induces autophagy in HCC. Autophagy is an intracellular regulatory mechanism that preserves cellular homeostasis by eliminating superfluous or dysfunctional cellular components and recycling metabolic substrates (19,20). To assess the effect of RPLP0 expression on autophagy levels in HCC, GSEA was conducted, revealing a statistically significant correlation between decreased RPLP0 expression and the augmentation of autophagic processes (Fig. 4A). Importantly, further validation through western blot analysis demonstrated that the suppression of RPLP0 resulted in a substantial elevation in the LC3B-II/LC3B-I ratio and a concurrent decrease in P62 levels (Fig. 4B). Subsequently, the presence of autophagosome vacuoles was evaluated employing MDC staining and transmission electron microscopy. The analysis unveiled that the downregulation of RPLP0 led to an increased accumulation of autophagosome vacuoles in HCC cells (Fig. 4C and D). Autophagy was inhibited by treating Huh7 and MHCC97-H cells that had been knocked down with 3-methyladenine (3-MA) (21). The outcomes signaled that 3-MA reversed the elevation in the LC3B-II/LC3B-I ratio induced by RPLP0 downregulation, indicating that RPLP0 knockdown indeed triggered autophagy (Fig. 5A). Given that the accumulation of autophagosomes may signify either enhanced autophagic

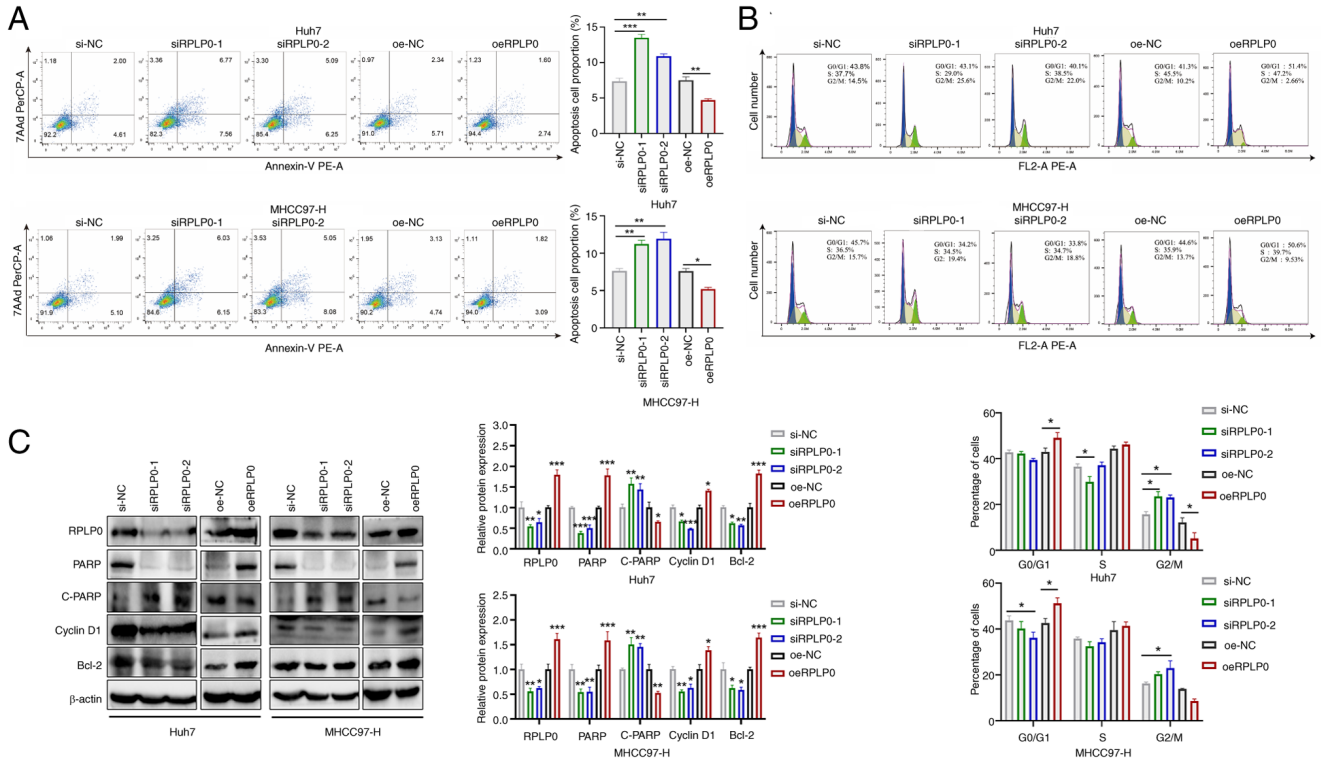

Figure 3. RPLP0 downregulation triggers apoptosis and G_2/M cell cycle arrest in HCC cells. Flow cytometry was performed to evaluate the (A) apoptosis rate and (B) cell cycle. (C) Western blotting was performed to quantify apoptosis- and cycle-related protein levels (C-PARP, PARP, Cyclin D1 and Bcl-2). *P<0.05, **P<0.01, ***P<0.001. RPLP0, ribosomal protein lateral stalk subunit P0; HCC, hepatocellular carcinoma; PARP, Poly (ADP-ribose) polymerase; C-, cleaved.

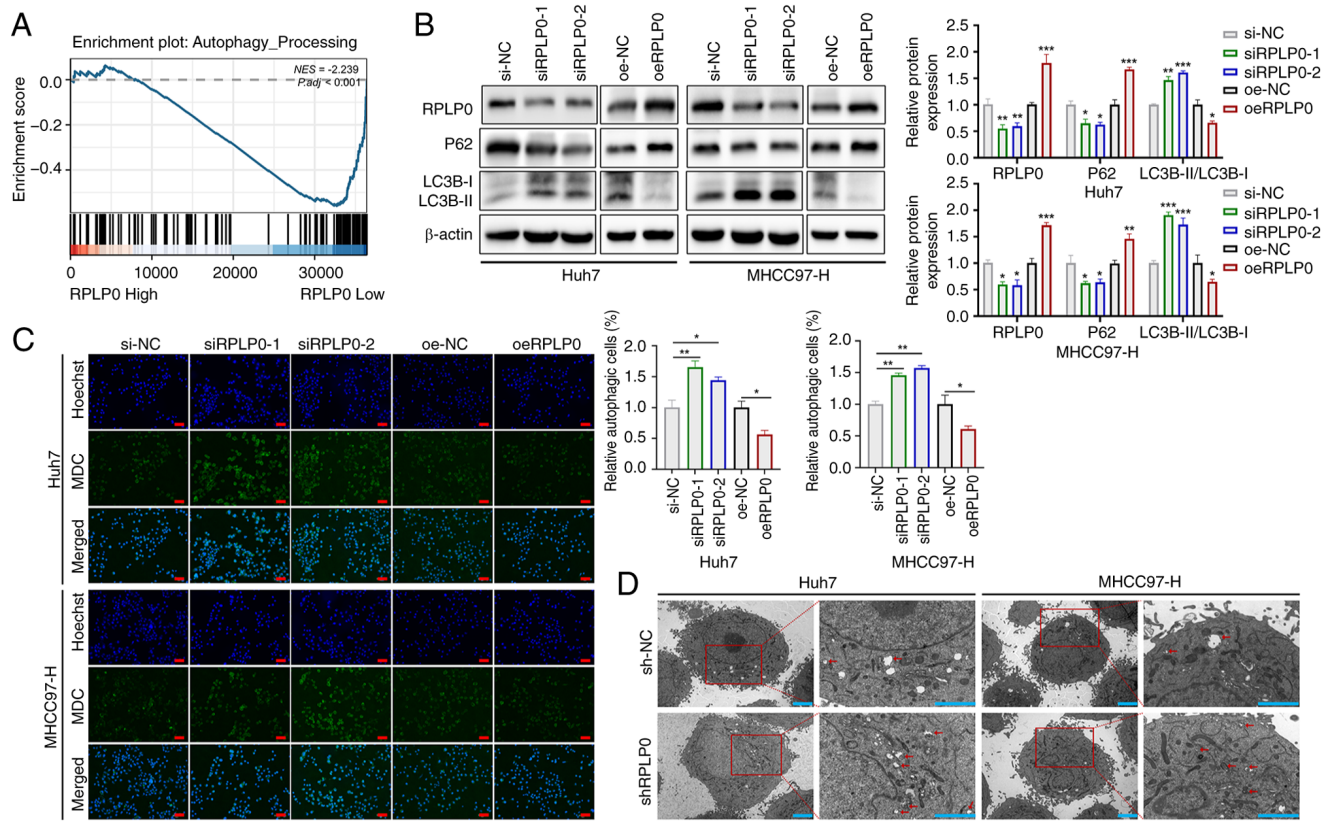

Figure 4. RPLP0 knockdown induces autophagy in HCC cells. (A) GSEA demonstrated a significant enrichment of low RPLP0 expression during autophagy. (B) Alterations in the levels of autophagy-related proteins (P62 and LC3B). (C) The presence of autophagosomes was assessed using MDC staining in HCC cells subjected to RPLP0 knockdown and overexpression (scale bar, 50 μm). (D) Autophagosome quantity was examined via transmission electron microscopy, with red arrows denoting autophagosomes (scale bar, 2 μm). *P<0.05, **P<0.01, ***P<0.001. RPLP0, ribosomal protein lateral stalk subunit P0; HCC, hepatocellular carcinoma; GSEA, gene set enrichment analysis; MDC, monodansylcadaverine.

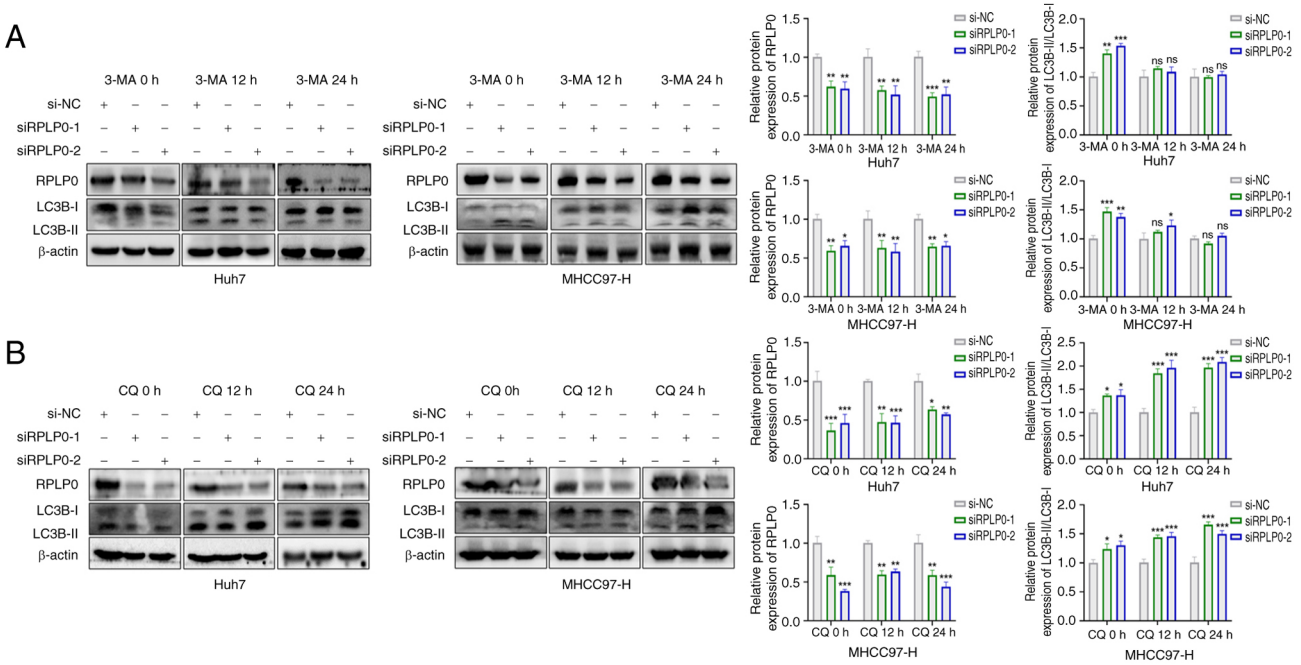

Figure 5. RPLP0 knockdown stimulates autophagic flux in HCC cells, as shown by 3-MA and CQ. (A) Western blotting analyzed LC3B expression in HCC cells pretreated with transfection and subsequently exposed to 5 mM 3-MA for 0, 12 and 24 h. (B) HCC cells were treated with 20 μM CQ for 0, 12 and 24 h, respectively, followed by RPLP0 knockdown, and western blotting evaluated LC3B levels. *P<0.05, **P<0.01, ***P<0.001. RPLP0, ribosomal protein lateral stalk subunit P0; HCC, hepatocellular carcinoma; 3-MA, 3-methyladenine; CQ, chloroquine.

flux or impaired autophagic processes (22), the effect of RPLP0 knockdown on autophagic flux was investigated by the administration of chloroquine (CQ), a known inhibitor of autophagy-lysosome fusion (23). Treatment with CQ resulted in an increase in the LC3B-II/LC3B-I ratio at both 12 and 24 h, suggesting that RPLP0 knockdown promoted autophagic flux (Fig. 5B). These findings unequivocally demonstrate that the downregulation of RPLP0 induces autophagy in HCC cells.

Suppression of RPLP0 expression impedes the progression of xenograft tumors. To explore the influence of RPLP0 knockdown on the progression of subcutaneous xenograft tumors, MHCC97-H cells were genetically modified using lentiviral vectors encoding either a non-targeting control short hairpin RNA (shNC) or an RPLP0-targeted short hairpin RNA (shRPLP0). Throughout the experimental period, the tumor volumes were meticulously monitored and documented at regular 4-day intervals. After 40 days, mouse xenograft models were successfully established, xenograft tumors were successfully isolated and tumor weights were statistically analyzed. The shRPLP0 group exhibited notably reduced tumor volumes and weights in comparison to the shNC group (Fig. 6A-D). Western blotting of excised tumors indicated that the shRPLP0 group demonstrated increased expression in E-cadherin and the LC3B-II/LC3B-I ratio relative to the shNC group. Meanwhile, the expression levels of Ki-67, Vimentin and Snail were markedly decreased in the shRPLP0 group (Fig. 6E). Furthermore, immunohistochemical analysis of the xenograft tumors demonstrated lower Ki-67 expression levels in the shRPLP0 group (Fig. 6F).

Suppression of RPLP0 inactivates the JAK2/STAT3 signaling pathway via ROS accumulation. Deficiency of the human ribosomal P complex in breast cancer has been shown to result in significant dysregulation of the TXN protein that neutralizes the effects of oxidative damage (9,24). As previously documented, RPLP0 knockdown promoted autophagy (Fig. 4A-D), which is closely related to intracellular oxidative stress (25,26). To explore the effect of RPLP0 knockdown on ROS production, GSEA was performed. The findings revealed significant enrichment of ROS accumulation in the low-RPLP0 expression group (Fig. 7A). DCFH-DA staining can directly reflect ROS levels (27). Accordingly, DCFH-DA staining was performed on transfected Huh7 and MHCC97-H cells and subsequent flow cytometry and fluorescence microscopy showed that RPLP0 knockdown markedly stimulated ROS production (Fig. 7B and C). To investigate the relationship between ROS and autophagy, ROS levels were decreased using N-acetyl-l-cysteine (NAC) (28). As depicted in Fig. 7D, a marked reduction in the LC3B-II/LC3B-I ratio was observed following 12 and 24 h of NAC treatment, suggesting that the progression of autophagy was contingent upon ROS production. Moreover, the results showed that RPLP0 knockdown inhibited JAK2/STAT3 pathway activation (Fig. 8A). IL-6 is well-documented as an activator of the JAK/STAT3 pathway (29-31). Following a 48-h transfection pretreatment in Huh7 and MHCC97-H cell lines, the administration of 40 ng/ml IL-6 for 24 h reverted alterations in RPLP0, phosphorylated (p-) JAK2/JAK2 and p-STAT3/STAT3 expression, implying that the activation of the JAK2/STAT3 pathway is at least partially dependent on RPLP0 (Fig. 8B). To further investigate the effects of RPLP0 knockdown on ROS-mediated alterations in the JAK2/STAT3 pathway, NAC was administered. The findings revealed that the levels of RPLP0, p-JAK2/JAK2 and p-STAT3/STAT3 exhibited time-dependent increases at 12 and 24 h post-treatment, suggesting that RPLP0

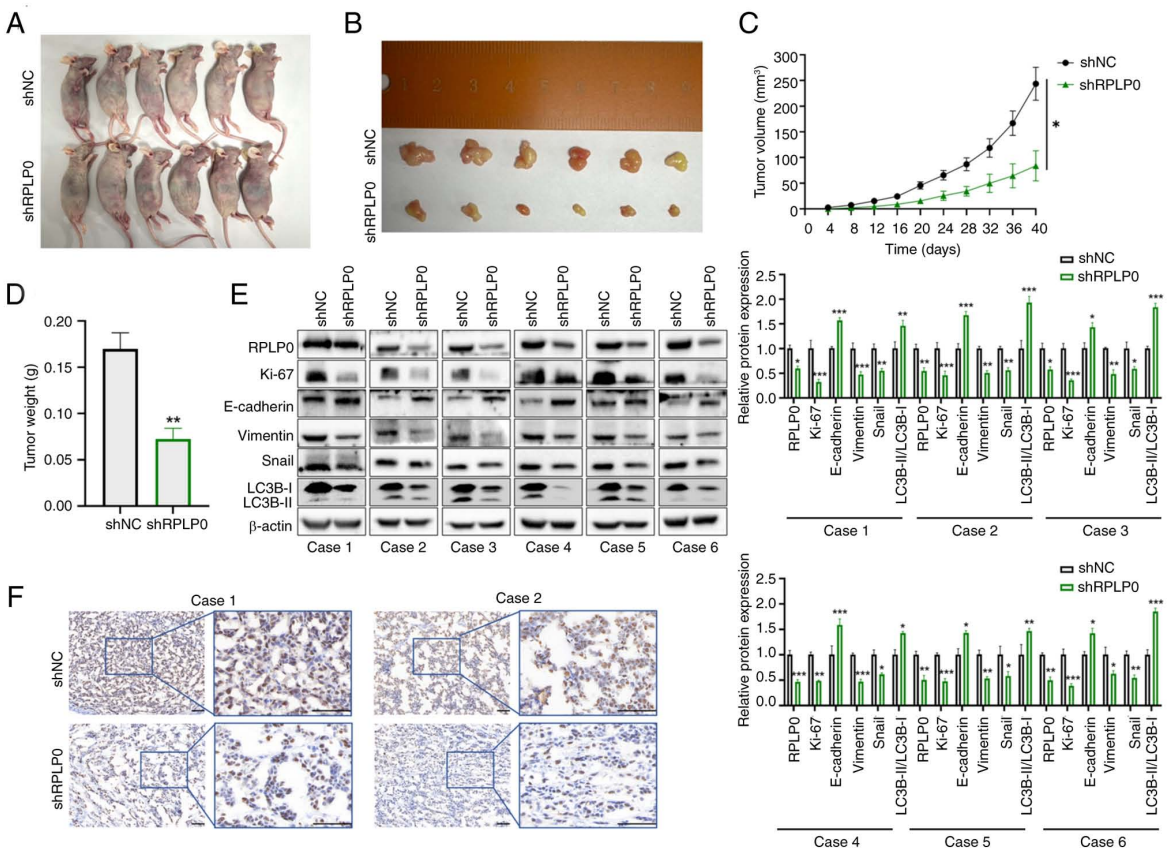

Figure 6. Suppression of RPLP0 expression impedes xenograft tumor growth. (A) Subcutaneous xenograft tumor models were established following pretreatment of MHCC97-H cells. (B) Xenograft tumors were successfully isolated. The (C) volume and (D) weight of subcutaneous xenografts were compared between the shNC and shRPLP0 groups. (E) Western blotting was performed to assess RPLP0, Ki-67, E-cadherin, Vimentin, Snail and LC3B levels in the xenografts. (F) Immunohistochemical staining for Ki-67 in the shNC and shRPLP0 groups (scale bar, 50 μm). *P<0.05, **P<0.01, ***P<0.001. RPLP0, ribosomal protein lateral stalk subunit P0; sh, short hairpin.

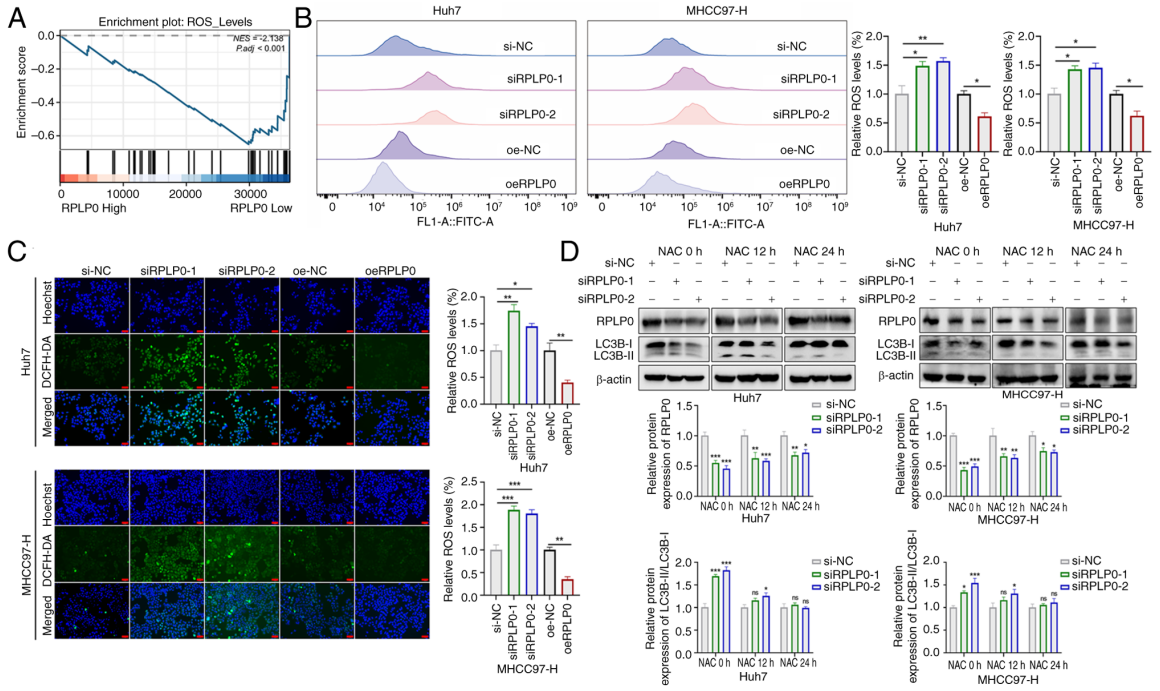

Figure 7. Suppression of RPLP0 expression promotes ROS accumulation. (A) GSEA demonstrated a significant correlation between reduced RPLP0 expression and increased ROS accumulation. (B) ROS levels were evaluated via flow cytometry following pretreatment. (C) Fluorescence microscopy was utilized to evaluate ROS levels (scale bar, 50 μm). (D) HCC cells were treated with 5 mM NAC for 0, 12 and 24 h and LC3B expression was analyzed via western blotting. *P<0.05, **P<0.01, ***P<0.001. RPLP0, ribosomal protein lateral stalk subunit P0; ROS, reactive oxygen species; GSEA, gene set enrichment analysis; HCC, hepatocellular carcinoma; NAC, N-acetyl-L-cysteine.

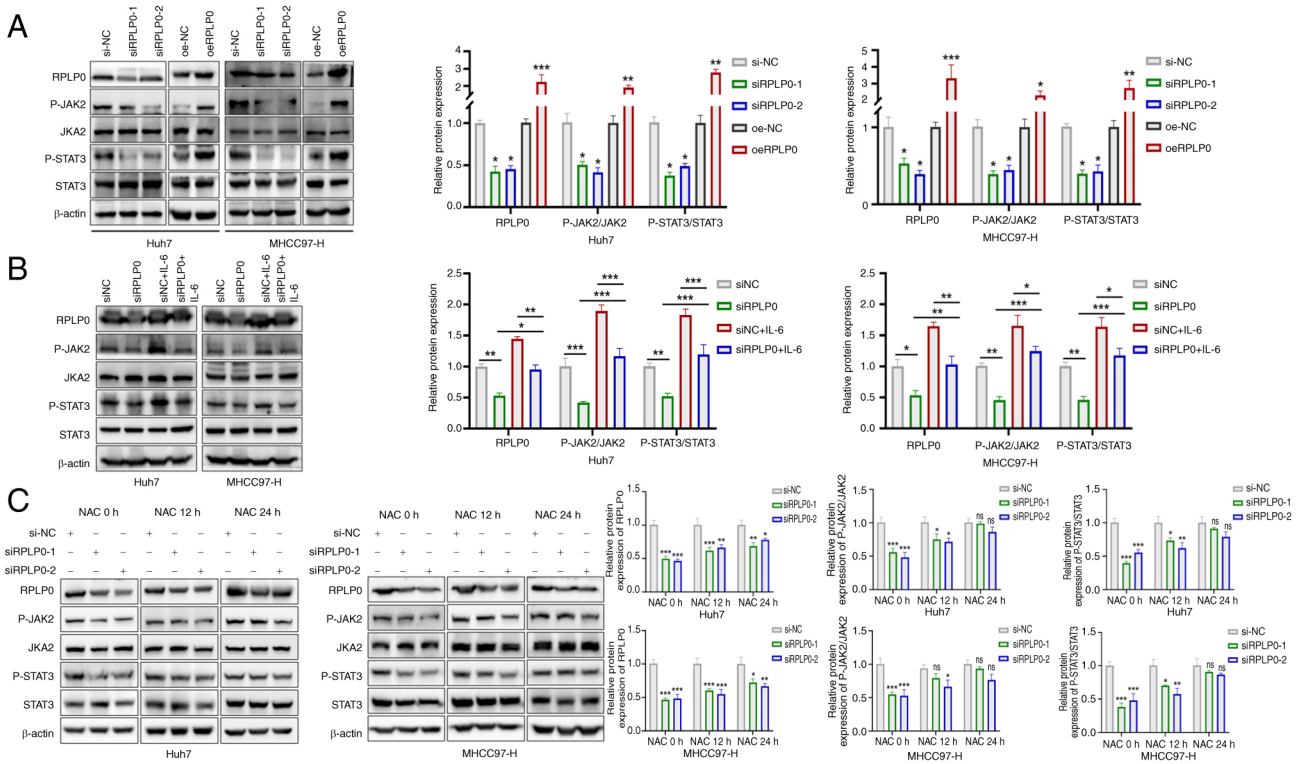

Figure 8. Suppressing RPLP0 deactivates the JAK2/STAT3 pathway by accumulating ROS. (A) Alterations in RPLP0, p-JAK2/JAK2 and p-STAT3/STAT3 expression were assessed in HCC cells following transfection. (B) After 48 h of transfection, Huh7 and MHCC97-H cells were exposed to 40 ng/ml IL-6 for an additional 24 h, followed by western blot analysis of RPLP0, p-JAK2/JAK2 and p-STAT3/STAT3 expression. (C) HCC cells underwent a 48-h transfection pretreatment and were then treated with 5 mM NAC for 0, 12 and 24 h, followed by western blot analysis of RPLP0, p-JAK2/JAK2 and p-STAT3/STAT3 expression. *P<0.05, **P<0.01, ***P<0.001. RPLP0, ribosomal protein lateral stalk subunit P0; ROS, reactive oxygen species; p-, phosphorylated; HCC, hepatocellular carcinoma; NAC, N-acetyl-L-cysteine.

knockdown induces ROS accumulation, which mediates the inactivation of the JAK2/STAT3 pathway (Fig. 8C). Notably, the mRNA levels of RPLP0 time-dependently increased following NAC treatment (Fig. S1). In summary, RPLP0 knockdown suppressed the JAK2/STAT3 signaling pathway by promoting ROS accumulation, consequently delaying the progression of HCC.

c-Myc activates RPLP0 transcription. To identify upstream regulators that activate RPLP0 transcription, predictions were made using the Cistrome Data Browser. As depicted in Fig. 9A, c-Myc had the highest relative score as a potential transcription factor for RPLP0. Correlation analyses of TCGA data and 44 HCC tissue samples demonstrated a statistically significant positive association between c-Myc and RPLP0 expression levels (Fig. 9B and C). Furthermore, c-Myc knockdown in HCC cells yielded a marked reduction in the mRNA and protein levels of both c-Myc and RPLP0 (Fig. 9D-F). The DNA binding motifs for c-Myc were retrieved from the JASPAR database and the corresponding primers (RPLP0-P1/P2/P3) were designed by selecting different binding sites with high relative scores (Fig. 9G). The direct interaction of c-Myc with the RPLP0 promoter region was validated through ChIP-qPCR and agarose gel electrophoresis of ChIP products (Fig. 9H and I). Moreover, luciferase reporter vectors for RPLP0-WT and RPLP0-MUT were constructed, incorporating specific c-Myc binding sites within the RPLP0 promoter sequence (Fig. 9J). The dual luciferase reporter assay results indicated that c-Myc enhanced the transcriptional activity of RPLP0-WT, whereas the luciferase activity of RPLP0-MUT remained unaffected by c-Myc (Fig. 9K). In summary, RPLP0 functioned as a direct target of c-Myc-mediated transcription.

RPLP0 facilitates the malignant progression of HCC through reliance on c-Myc regulation. To investigate whether the involvement of RPLP0 in advancing HCC development is contingent upon c-Myc regulation, Huh7 and MHCC97-H cell lines were used in co-transfection experiments. Downregulation of c-Myc reversed the increases in HCC cell proliferation, invasion and migration induced by RPLP0 overexpression (Fig. 10A-C). Furthermore, RPLP0 overexpression restored the levels of Vimentin and Snail while concomitantly downregulating E-cadherin expression (Fig. 10D). Flow cytometry analysis revealed that c-Myc knockdown effectively mitigated the suppression of apoptosis and the G_2/M cell cycle arrest induced by RPLP0 overexpression (Fig. 11A and B). In addition, western blot analysis revealed that downregulation of c-Myc partially counteracted the influence of RPLP0 overexpression on the protein levels of PARP, C-PARP, Cyclin D1 and Bcl-2, as well as the LC3B-II/LC3B-I ratio (Fig. 11C). The present observations provide supporting evidence for the involvement of RPLP0 in facilitating HCC progression, with modulation of c-Myc serving as a key mechanism in this process. Collectively, these results indicate that RPLP0, regulated by c-Myc, activates the JAK2/STAT3 signaling pathway by reducing ROS levels, thereby facilitating the malignant progression of HCC (Fig. 12).

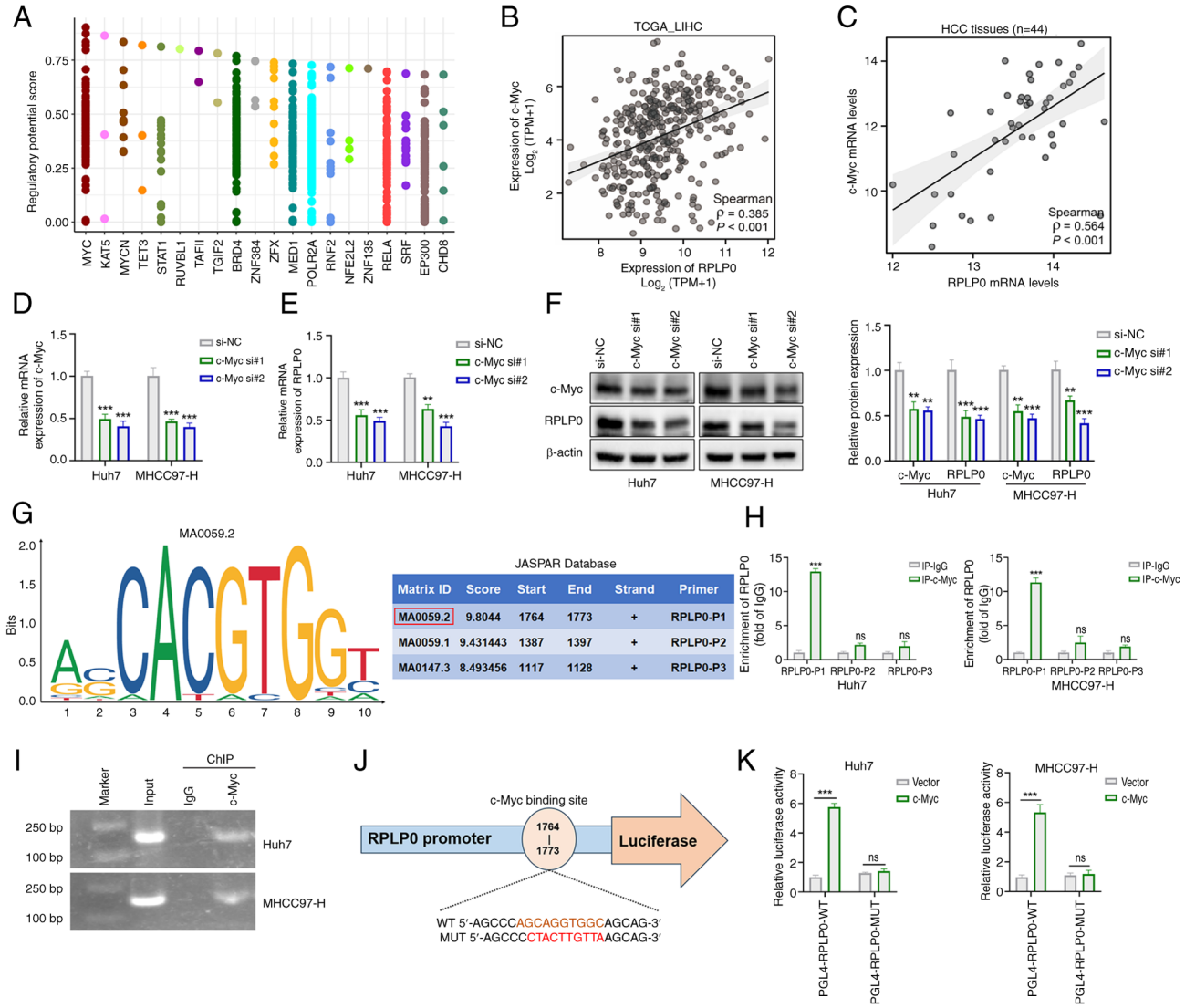

Figure 9. c-Myc promotes RPLP0 transcription. (A) The Cistrome Data Browser database was used to predict transcription factors associated with RPLP0. Correlation analyses of RPLP0 and c-Myc expression were conducted from the (B) TCGA database and (C) HCC samples (n=44). (D) HCC cells were transfected for 24 h to evaluate the knockdown efficiency of c-Myc mRNA and (E) the corresponding expression level of RPLP0 mRNA. (F) HCC cells were transfected for 48 h to examine alterations in c-Myc and RPLP0 protein expression. (G) A schematic illustration of c-Myc binding motifs, along with the relative scoring of binding sites derived from the JASPAR database. Corresponding primers were designed based on these binding sites. (H) ChIP-qPCR was conducted to investigate the binding of c-Myc to RPLP0 promoter sequences. (I) Agarose gel electrophoresis was performed to visualize the binding of c-Myc to RPLP0 promoter sequences (input as a positive control, IgG as a negative control). (J) Identification of potential sites for c-Myc binding to the RPLP0 promoter region. (K) HCC cells were co-transfected and subsequently analyzed for luciferase activity. **P<0.01, ***P<0.001. RPLP0, ribosomal protein lateral stalk subunit P0; HCC, hepatocellular carcinoma; ChIP, chromatin immunoprecipitation; qPCR, quantitative polymerase chain reaction.

Discussion

Oncogene activation and tumor suppressor gene inactivation are critical determinants in the malignant progression of HCC (32,33). The aberrant activation of pro-carcinogenic genes can drive the abnormal proliferation and malignant transformation of hepatocytes (34,35). Consequently, a pressing requirement exists to discover potential biological markers for diagnostic and prognostic evaluation. The present study comprehensively analyzed bioinformatics databases, diverse HCC cell lines and tissue samples and concluded that elevated RPLP0 levels in HCC are closely linked to unfavorable patient prognosis. These findings indicated that RPLP0 may function as a tumorigenic factor in HCC progression. A series of functional experiments on HCC cells showed that downregulating RPLP0 expression substantially hindered cellular proliferation, invasion and migration capabilities and induced G_2/M cell cycle arrest, along with the triggering of apoptotic and autophagic processes. The results of analogous xenograft tumor experiments indicated that the knockdown of RPLP0 effectively suppressed tumor growth.

Cellular autophagy can be induced by a range of factors, such as organelle damage, nutritional deficiencies and oxidative stress (36). ROS functions as highly reactive oxygenates and their excessive production leads to cell cycle arrest and mitochondria-dependent apoptosis (37). The present investigation revealed that the reduction of RPLP0 expression facilitated the accumulation of ROS, supported by the results of both GSEA analysis and DCFH-DA staining. In addition, the results indicated that RPLP0 knockdown inhibited JAK2/STAT3 pathway

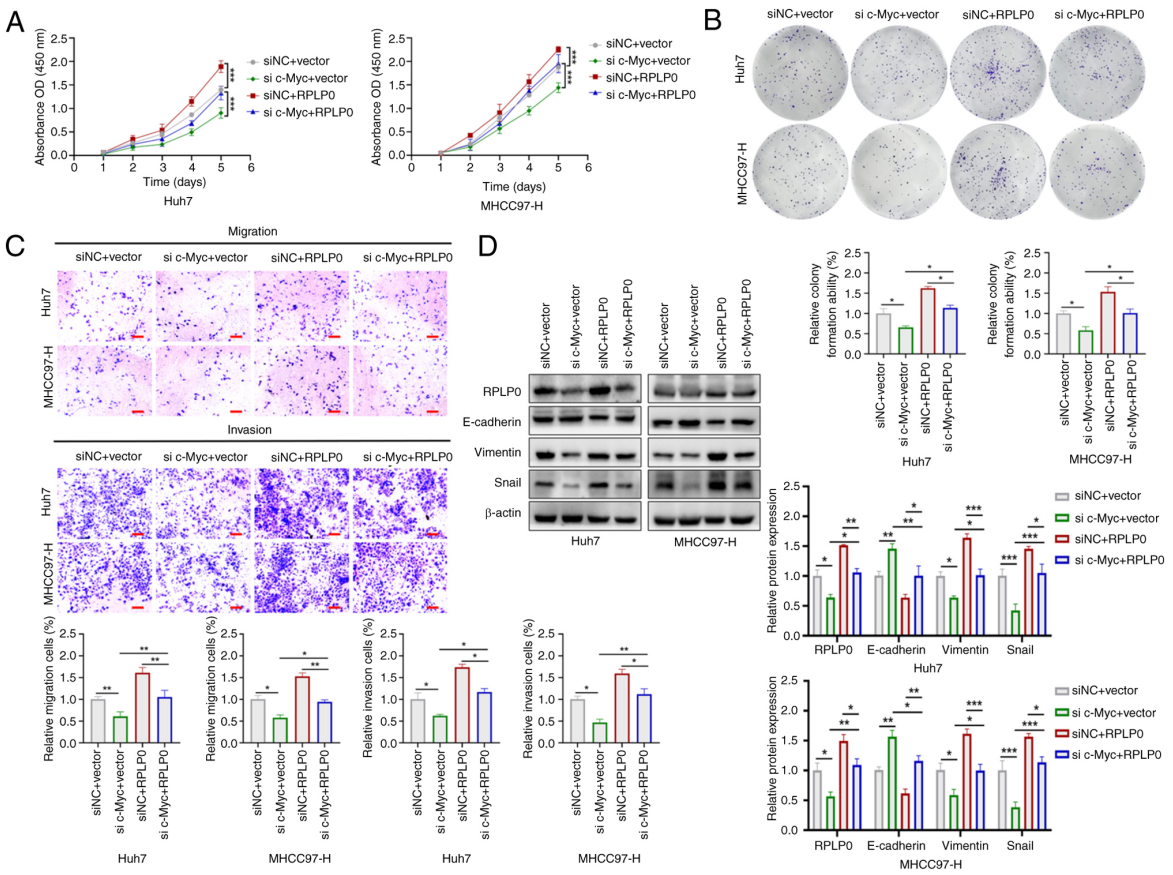

Figure 10. RPLP0 facilitates the proliferation and metastasis of HCC cells through the regulation of c-Myc. (A) CCK-8, (B) colony formation and (C) Transwell assays were used to assess cell proliferation, migration and invasion (scale bar, 150 μm). (D) EMT-related protein levels, such as E-cadherin, Vimentin and Snail, were examined in co-transfected HCC cells. *P<0.05, **P<0.01, ***P<0.001. RPLP0, ribosomal protein lateral stalk subunit P0; HCC, hepatocellular carcinoma; EMT, epithelial-mesenchymal transition.

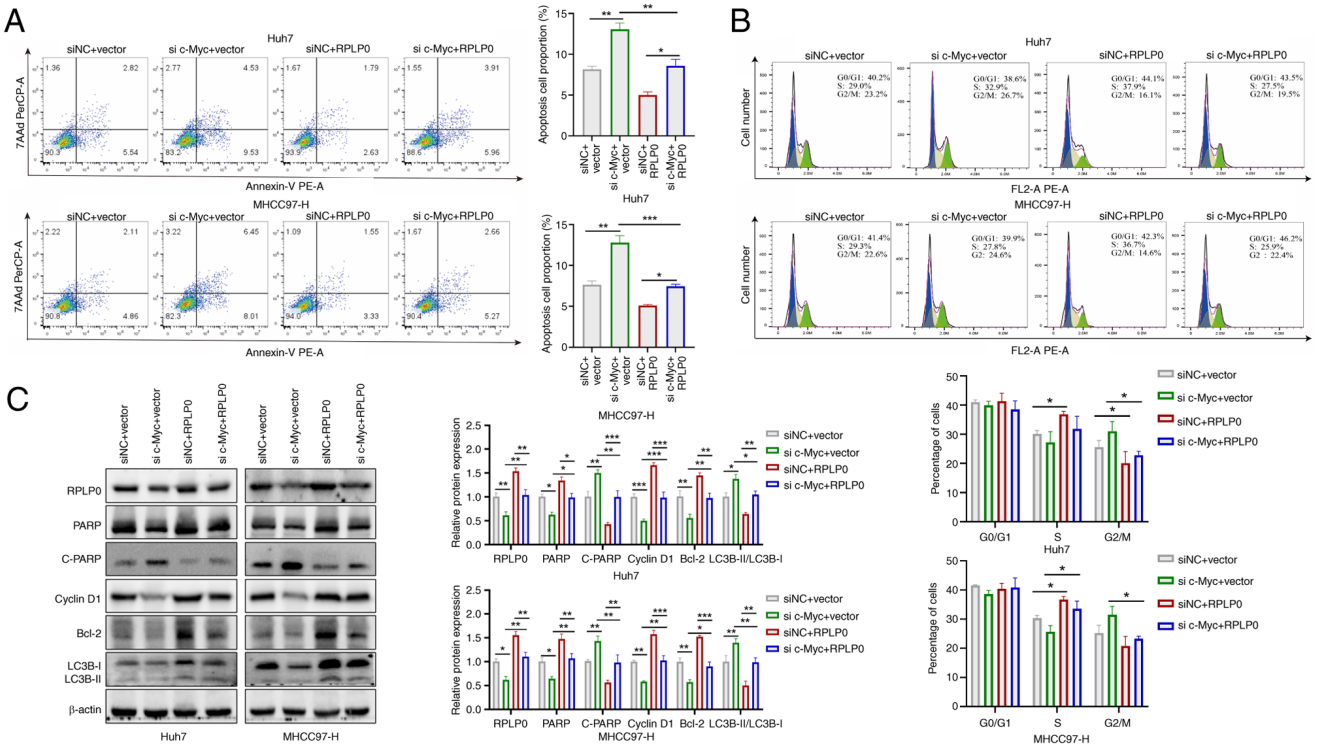

Figure 11. RPLP0-mediated regulation of apoptosis and cell cycle distribution in HCC cells depends on c-Myc. The (A) apoptosis rate and (B) cell cycle distribution were analyzed via flow cytometry. (C) Western blotting was used to evaluate PARP, C-PARP, Cyclin D1, Bcl-2 and LC3B expression. *P<0.05, **P<0.01, ***P<0.001. RPLP0, ribosomal protein lateral stalk subunit P0; HCC, hepatocellular carcinoma; PARP, Poly (ADP-ribose) polymerase; C-, cleaved.

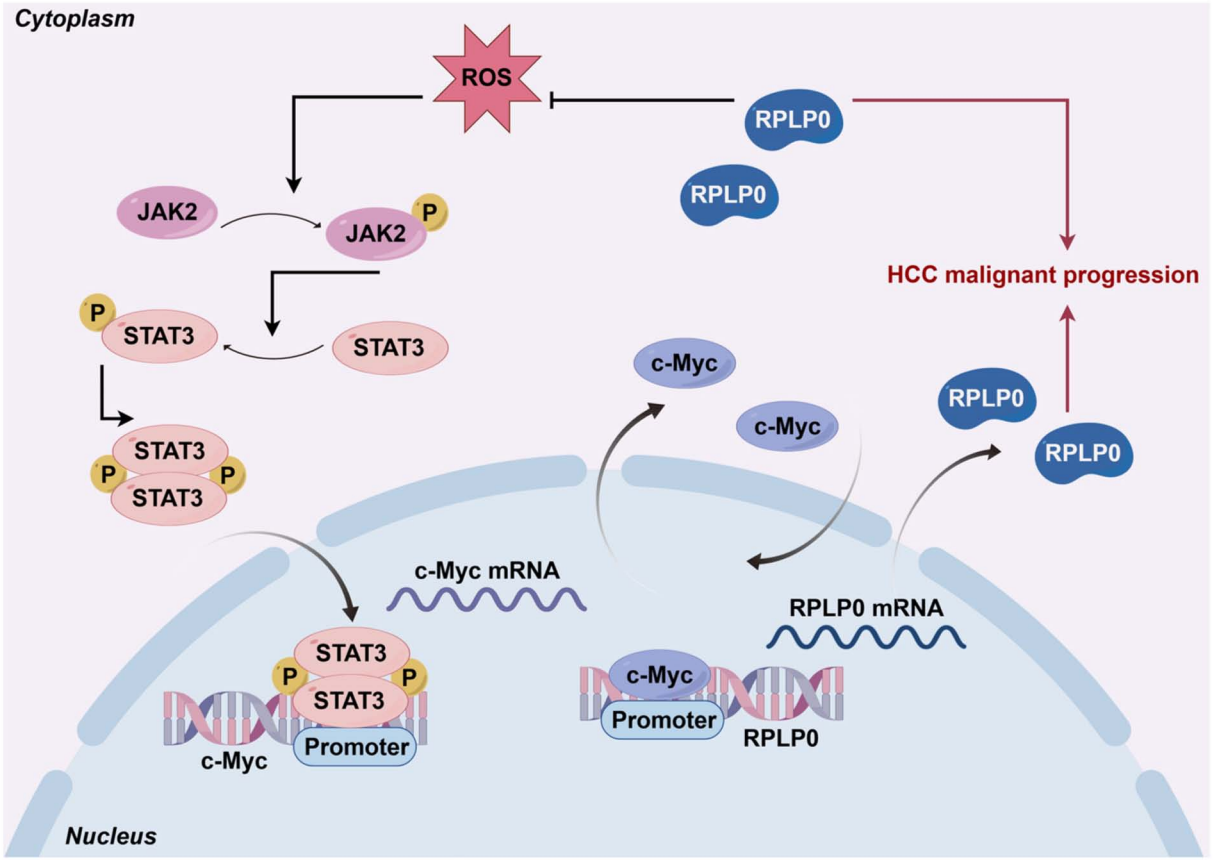

Figure 12. RPLP0, regulated by c-Myc, facilitates HCC progression by reducing ROS levels and activating the JAK2/STAT3 signaling pathway. Functional model of the c-Myc/RPLP0/ROS/JAK2/STAT3 signaling axis. RPLP0, ribosomal protein lateral stalk subunit P0; HCC, hepatocellular carcinoma; ROS, reactive oxygen species.

activation. Subsequently, in-depth investigations revealed that the supplementation of NAC, following the knockdown of RPLP0, time-dependently increased RPLP0, p-JAK2/JAK2 and p-STAT3/STAT3 levels, suggesting that RPLP0 silencing mediates JAK2/STAT3 signaling pathway inactivation by increasing ROS levels. Prior investigations have identified a significant association between elevated ROS concentrations and the suppression of the JAK2/STAT3 pathway, accompanied by increased autophagic activity (38-42). In the present study, RPLP0 knockdown resulted in increased ROS levels, which in turn repressed JAK2/STAT3 pathway activation and stimulated autophagic processes, consequently impeding the malignant progression of HCC.

Notably, both mRNA and protein levels of RPLP0 exhibited a time-dependent upregulation following the administration of NAC at 12 and 24 h, suggesting that RPLP0 may be regulated by transcription factors. Furthermore, the present study demonstrated that NAC effectively counteracted the downregulation in p-JAK2/JAK2 and p-STAT3/STAT3 expression induced by RPLP0 knockdown. Previous investigations have established that p-STAT3 possesses the ability to translocate into the nucleus, modulating the transcription of various target genes, such as c-Myc, BCL-2, Vimentin and MMP2/9, among others (43-45). It is worthwhile emphasizing that the Cistrome Data Browser database was used to predict potential transcription factors for RPLP0 and the results demonstrated that c-Myc exhibited the highest relative score. An in-depth analysis of data sourced from TCGA database, coupled with an examination of HCC tissue samples, revealed a significant positive correlation between the expression levels of RPLP0 and c-Myc. As a prevalent oncogene, c-Myc facilitates the onset and progression of various tumors by enhancing cellular growth and proliferation, modulating the transcription of downstream target genes, inducing genomic instability and reprogramming cellular metabolism (46-48). Subsequently, CHIP and dual luciferase reporter assays revealed that c-Myc interacts with the promoter sequence of RPLP0 to promote its transcription.

The present study demonstrated that RPLP0 knockdown elevated intracellular ROS levels, thereby inducing autophagy. However, the precise molecular mechanisms by which RPLP0 regulates ROS generation remain unclear. Elucidating the upstream signals and downstream effectors of RPLP0-mediated oxidative stress is a key objective of our ongoing research.

In summary, the present study offered a new perspective on the function of RPLP0 as a pro-oncogenic factor in the progression of HCC. The results indicated that RPLP0 forms a feedback loop with c-Myc via the ROS-mediated JAK2/STAT3 pathway. Concurrently, c-Myc reciprocally activates RPLP0, thereby perpetuating the circuit and contributing to the progression of HCC. The findings of the present study provided innovative perspectives on potential therapeutic approaches for the management of HCC.

Acknowledgments

The authors wish to express their sincere gratitude to Professor Fanglin Zheng, Institute of Respiratory Diseases, The First Affiliated Hospital, Jiangxi Medical College, Nanchang University, for his invaluable advice.

Funding

The present study was supported by Jiangxi Kang-shen Biotechnology Company (grant no. 1210702001), Wu Jieping Medical Foundation (grant no. 320.6750.2024-13-32) and the Innovative and Entrepreneurial Youth Talents Project of Jiangxi (grant no. JXSQ2018106040).

Availability of data and materials

The data generated in the present study are included in the figures and/or tables of this article.

Authors' contributions

YQM and LBY conceived and designed the study. GRM, HXH, and XBH performed most of the experiments, analyzed the data, and wrote the manuscript. XPX and XDP supervised the entire project. YQM and XDP confirm the authenticity of all raw data. All authors read and approved the final manuscript.

Ethics approval and consent to participate

The present study was approved by the Ethics Committee of the First Affiliated Hospital of Nanchang University approval no. (2024)CDYFYYLK (07-004) and all patients provided informed consent. The animal experiments were also approved by the animal ethics committee (approval no. CDYFY-IACUC-202407QR259).

Patient consent for publication

Not applicable.

Competing interests

The authors declare that they have no competing interests.

References

1. Bray F, Laversanne M, Sung H, Ferlay J, Siegel RL, Soerjomataram I and Jemal A: Global cancer statistics 2022: GLOBOCAN estimates of incidence and mortality worldwide for 36 cancers in 185 countries. CA Cancer J Clin 74: 229-263, 2024.
2. Wang X, Zhang L and Dong B: Molecular mechanisms in MASLD/MASH-related HCC. Hepatology 8: 1303-1324, 2025.
3. Foerster F, Gairing SJ, Müller L and Galle PR: NAFLD-driven HCC: Safety and efficacy of current and emerging treatment options. J Hepatol 76: 446-457, 2022.
4. Toh MR, Wong EYT, Wong SH, Ng AWT, Loo LH, Chow PK and Ngeow J: Global epidemiology and genetics of hepatocellular carcinoma. Gastroenterology 164: 766-782, 2023.
5. Childs A, Aidoo-Micah G, Maini MK and Meyer T: Immunotherapy for hepatocellular carcinoma. JHEP Rep 6: 101130, 2024.
6. Medavaram S and Zhang Y: Emerging therapies in advanced hepatocellular carcinoma. Exp Hematol Oncol 7: 17, 2018.
7. Rimassa L, Pressiani T and Merle P: Systemic treatment options in hepatocellular carcinoma. Liver Cancer 8: 427-446, 2019.
8. Artero-Castro A, Castellvi J, García A, Hernández J, Ramón Y Cajal S and Lleonart ME: Expression of the ribosomal proteins Rplp0, Rplp1, and Rplp2 in gynecologic tumors. Hum Pathol 42: 194-203, 2011.
9. Artero-Castro A, Perez-Alea M, Feliciano A, Leal JA, Genestar M, Castellvi J, Peg V, Ramón Y Cajal S and Lleonart ME: Disruption of the ribosomal P complex leads to stress-induced autophagy. Autophagy 11: 1499-1519, 2015.
10. Teller A, Jechorek D, Hartig R, Adolf D, Reißig K, Roessner A and Franke S: Dysregulation of apoptotic signaling pathways by interaction of RPLP0 and cathepsin X/Z in gastric cancer. Pathol Res Pract 211: 62-70, 2015.
11. Wang CH, Wang LK, Wu CC, Chen ML, Lee MC, Lin YY and Tsai FM: The ribosomal protein RPLP0 mediates PLAAT4-induced cell cycle arrest and cell apoptosis. Cell Biochem Biophys 77: 253-260, 2019.
12. Wang YL, Zhao WW, Bai SM, Ma Y, Yin XK, Feng LL, Zeng GD, Wang F, Feng WX, Zheng J, *et al*: DNA damage-induced paraspeckle formation enhances DNA repair and tumor radioresistance by recruiting ribosomal protein P0. Cell Death Dis 13: 709, 2022.
13. Debnath J, Gammoh N and Ryan KM: Autophagy and autophagy-related pathways in cancer. Nat Rev Mol Cell Biol 24: 560-575, 2023.
14. Miller DR and Thorburn A: Autophagy and organelle homeostasis in cancer. Dev Cell 56: 906-918, 2021.
15. Meng Y, Huang X, Zhang G, Fu S, Li Y, Song J, Zhu Y, Xu X and Peng X: MicroRNA-450b-5p modulated RPLP0 promotes hepatocellular carcinoma progression via activating JAK/STAT3 pathway. Transl Oncol 50: 102150, 2024.
16. Zheng P, Xu D, Cai Y, Zhu L, Xiao Q, Peng W and Chen B: A multi-omic analysis reveals that Gamabufotalin exerts anti-hepatocellular carcinoma effects by regulating amino acid metabolism through targeting STAMBPL1. Phytomedicine 135: 156094, 2024.
17. Livak KJ and Schmittgen TD: Analysis of relative gene expression data using real-time quantitative PCR and the 2(-Delta Delta C(T)) method. Methods 25: 402-408, 2001.
18. Qian J, Wang Q, Xiao L, Xiong W, Xian M, Su P, Yang M, Zhang C, Li Y, Zhong L, *et al*: Development of therapeutic monoclonal antibodies against DKK1 peptide-HLA-A2 complex to treat human cancers. J Immunother Cancer 12: e008145, 2024.
19. Mizushima N and Komatsu M: Autophagy: Renovation of cells and tissues. Cell 147: 728-741, 2011.
20. Mizushima N and Levine B: Autophagy in human diseases. N Engl J Med 383: 1564-1576, 2020.
21. Yan LS, Zhang SF, Luo G, Cheng BC, Zhang C, Wang YW, Qiu XY, Zhou XH, Wang QG, Song XL, *et al*: Schisandrin B mitigates hepatic steatosis and promotes fatty acid oxidation by inducing autophagy through AMPK/mTOR signaling pathway. Metabolism 131: 155200, 2022.
22. Zhao YG, Codogno P and Zhang H: Machinery, regulation and pathophysiological implications of autophagosome maturation. Nat Rev Mol Cell Biol 22: 733-750, 2021.
23. Miao CC, Hwang W, Chu LY, Yang LH, Ha CT, Chen PY, Kuo MH, Lin SC, Yang YY, Chuang SE, *et al*: LC3A-mediated autophagy regulates lung cancer cell plasticity. Autophagy 18: 921-934, 2022.
24. Bradford HF, McDonnell TCR, Stewart A, Skelton A, Ng J, Baig Z, Fraternali F, Dunn-Walters D, Isenberg DA, Khan AR, *et al*: Thioredoxin is a metabolic rheostat controlling regulatory B cells. Nat Immunol 25: 873-885, 2024.
25. Ornatowski W, Lu Q, Yegambaram M, Garcia AE, Zemskov EA, Maltepe E, Fineman JR, Wang T and Black SM: Complex interplay between autophagy and oxidative stress in the development of pulmonary disease. Redox Biol 36: 101679, 2020.
26. Russell RC and Guan KL: The multifaceted role of autophagy in cancer. EMBO J 41: e110031, 2022.
27. Yang R, Gao W, Wang Z, Jian H, Peng L, Yu X, Xue P, Peng W, Li K and Zeng P: Polyphyllin I induced ferroptosis to suppress the progression of hepatocellular carcinoma through activation of the mitochondrial dysfunction via Nrf2/HO-1/GPX4 axis. Phytomedicine 122: 155135, 2024.
28. Tsai HY, Bronner MP, March JK, Valentine JF, Shroyer NF, Lai LA, Brentnall TA, Pan S and Chen R: Metabolic targeting of NRF2 potentiates the efficacy of the TRAP1 inhibitor G-TPP through reduction of ROS detoxification in colorectal cancer. Cancer Lett 549: 215915, 2022.

29. Johnson DE, O'Keefe RA and Grandis JR: Targeting the IL-6/JAK/STAT3 signalling axis in cancer. Nat Rev Clin Oncol 15: 234-248, 2018.
30. Lai SY and Johnson FM: Defining the role of the JAK-STAT pathway in head and neck and thoracic malignancies: Implications for future therapeutic approaches. Drug Resist Updat 13: 67-78, 2010.
31. Yu H, Lee H, Herrmann A, Buettner R and Jove R: Revisiting STAT3 signalling in cancer: new and unexpected biological functions. Nat Rev Cancer 14: 736-746, 2014.
32. Chen L, Zhang C, Xue R, Liu M, Bai J, Bao J, Wang Y, Jiang N, Li Z, Wang W, *et al*: Deep whole-genome analysis of 494 hepatocellular carcinomas. Nature 627: 586-593, 2024.
33. Ng CKY, Dazert E, Boldanova T, Coto-Llerena M, Nuciforo S, Ercan C, Suslov A, Meier MA, Bock T, Schmidt A, *et al*: Integrative proteogenomic characterization of hepatocellular carcinoma across etiologies and stages. Nat Commu 13: 2436, 2022.
34. Calderaro J, Ziol M, Paradis V and Zucman-Rossi J: Molecular and histological correlations in liver cancer. J Hepatol 71: 616-630, 2019.
35. Villanueva A: Hepatocellular carcinoma. N Engl J Med 380: 1450-1462, 2019.
36. Li X, He S and Ma B: Autophagy and autophagy-related proteins in cancer. Mol Cancer 19: 12, 2020.
37. Fan J, Ren D, Wang J, Liu X, Zhang H, Wu M and Yang G: Bruceine D induces lung cancer cell apoptosis and autophagy via the ROS/MAPK signaling pathway in vitro and in vivo. Cell Death Dis 11: 126, 2020.
38. Cao Y, Wang J, Tian H and Fu GH: Mitochondrial ROS accumulation inhibiting JAK2/STAT3 pathway is a critical modulator of CYT997-induced autophagy and apoptosis in gastric cancer. J Exp Clin Cancer Res 39: 119, 2020.
39. Kim J, Park A, Hwang J, Zhao X, Kwak J, Kim HW, Ku M, Yang J, Kim TI, Jeong KS, *et al*: KS10076, a chelator for redox-active metal ions, induces ROS-mediated STAT3 degradation in autophagic cell death and eliminates ALDH1+ stem cells. Cell Rep 40: 111077, 2022.
40. Liang JR and Yang H: Ginkgolic acid (GA) suppresses gastric cancer growth by inducing apoptosis and suppressing STAT3/JAK2 signaling regulated by ROS. Biomed Pharmacother 125: 109585, 2020.
41. Zhao Z, Wang Y, Gong Y, Wang X, Zhang L, Zhao H, Li J, Zhu J, Huang X, Zhao C, *et al*: Celastrol elicits antitumor effects by inhibiting the STAT3 pathway through ROS accumulation in non-small cell lung cancer. J Transl Med 20: 525, 2022.
42. Zhou H, Li J, He Y, Xia X, Liu J and Xiong H: SLC25A17 inhibits autophagy to promote triple-negative breast cancer tumorigenesis by ROS-mediated JAK2/STAT3 signaling pathway. Cancer Cell Int 24: 85, 2024.
43. Garg M, Shanmugam MK, Bhardwaj V, Goel A, Gupta R, Sharma A, Baligar P, Kumar AP, Goh BC, Wang L and Sethi G: The pleiotropic role of transcription factor STAT3 in oncogenesis and its targeting through natural products for cancer prevention and therapy. Med Res Rev: December 1, 2020 Epub ahead of print.
44. Hu Y, Dong Z and Liu K: Unraveling the complexity of STAT3 in cancer: Molecular understanding and drug discovery. J Exp Clin Cancer Res 43: 23, 2024.
45. Zou S, Tong Q, Liu B, Huang W, Tian Y and Fu X: Targeting STAT3 in cancer immunotherapy. Mol Cancer 19: 145, 2020.
46. Dhanasekaran R, Deutzmann A, Mahauad-Fernandez WD, Hansen AS, Gouw AM and Felsher DW: The MYC oncogene-the grand orchestrator of cancer growth and immune evasion. Nat Rev Clin Oncol 19: 23-36, 2022.
47. Duffy MJ, O'Grady S, Tang M and Crown J: MYC as a target for cancer treatment. Cancer Treat Rev 94: 102154, 2021.
48. Lourenco C, Resetca D, Redel C, Lin P, MacDonald AS, Ciaccio R, Kenney TMG, Wei Y, Andrews DW, Sunnerhagen M, *et al*: MYC protein interactors in gene transcription and cancer. Nat Rev Cancer 21: 579-591, 2021.